Effect of Oxygen Vacancy on Phase Transition and Photoluminescence Properties of Nanocrystalline Zirconia Synthesized by the One-Pot Reaction

Yan Cong,[†,§] Bin Li,[*,†] Shumei Yue,[†] and Di Fan[†]

Key Laboratory of Excited State Processes, Changchun Institute of Optics, Fine Mechanics and Physics, Chinese Academy of Sciences, Changchun, 130033, P.R. China and Graduate School of the Chinese Academy of Sciences, Chinese Academy of Sciences, Beijing, 100039, China

Xiao-jun Wang*[,‡]

Department of Physics, Georgia Southern University, Statesboro, Georgia 30460

Received: November 25, 2008; Revised Manuscript Received: March 2, 2009

Nanocrystalline ZrO_2 fine powders were prepared via the one-pot reaction followed by annealing from 700 to 1100 °C in air. It is believed that generation of excess oxygen vacancies within nanocrystalline ZrO_2 is primarily responsible for room-temperature tetragonal phase stabilization below a critical size, and the phase transformation from tetragonal to monoclinic ZrO_2 happened in the annealing process. Luminescent properties of ZrO_2 were greatly affected by oxygen vacancies in the phase transition process. Two bands centered at 350 and 470 nm were observed in tetragonal ZrO_2. The electrons trapped by oxygen vacancies creating F centers recombined with holes yielding the 350 nm luminescence. Temporal decay of the 470 nm luminescence is due to the detrapping of electrons to the Ti^{3+} luminescence centers. Elevated temperature accelerated the phase transformation to monoclinic ZrO_2 and decreased the oxygen vacancy concentration, resulting in a decrease of the 350 nm emission and enhancement of the 470 nm phosphorescence.

1. Introduction

Zirconia (ZrO_2) is a wide band gap (5.0−5.5 eV) transition metal oxide with useful mechanical, thermal, optical, and electrical properties. It has a variety of applications, including solid-state electrolytes, thermal barrier coatings, electro−optical materials, and oxygen sensors.[1−3] ZrO_2 exhibits three crystallographic phases with increasing temperature at a normal atmospheric pressure: the monoclinic phase, from room temperature to 1175 °C; the tetragonal phase, from 1175 to 2370 °C; and the cubic phase, from 2370 to 2750 °C (melting point).[4] However, the tetragonal and cubic phases can be stabilized at room temperature by doping yttrium, magnesium, and calcium oxides, and generating oxygen ion vacancies. Generally, it is these modifications (vacancies and changes in geometric and electronic structures) that lead to the useful transport, chemical, and optical properties of doped zirconia.[5,6]

Many properties of nanocrystalline zirconia are fundamentally different from those of conventional micrometer-sized zirconia because of the small crystallite dimension.[7,8] They exhibit increased strength and ductility, enhanced diffusivity, and increased edges and corners, all beneficial for applications in catalysis, electronics, and ceramics. Particle size has also been observed to have an effect on the metastable tetragonal phase stability in nanocrystalline zirconia.[9,10] Defect vacancies are thought to be the most important influencing factor of phase stability. The tetragonal phase can be stabilized at room temperature below a critical size, which is due to the generation of excess oxygen vacancies as a result of the size effect. Oxygen ion vacancies are primarily responsible for the stability of the phase structure and phase transformation of zirconia. They serve as F centers and electron traps, which also greatly affect the luminescent properties in ZrO_2.[11]

Many synthesis routes have been proposed for the preparation of nanocrystalline ZrO_2 powders and colloids. Among them, the sol−gel process is one of the most frequently utilized methods.[12] However, zirconium alkoxides, the sol−gel precursors for ZrO_2, are expensive, unavailable, and toxic, and it is difficult to control the homogeneity of different components. Anionic surfactants have also been used to synthesize nanocrystalline ZrO_2, but a disordered product was obtained.[13] Zhao and co-workers synthesized very ordered nanosized ZrO_2 in a nonaqueous solution.[14] Polyzirconoxane (PZO) consists of a main chain of Zr−O bonds with ethyl acetoacetate (Hetac) and OH groups as a pendant. Immobilization of Zr and O in such a polymeric long-chain structure ensures compositional homogeneity. Nanocrystalline ZrO_2 can be synthesized using PZO as an ordered structure, but it is not practical because PZO has to be prepared via the synthetic processes of zirconium tetraalkoxide and the zirconium chelate complex. In this paper, a convenient one-pot reaction method is reported to synthesize PZO by reacting zirconium oxychloride with the Hetac in the presence of triethylamine. PZO is sintered in different temperatures to form nanocrystalline ZrO_2. Their luminescence properties and crystalline structure characterizations are also studied as a function of the annealing temperature. The tetragonal phase is stabilized at room temperature due to the generation of excess oxygen vacancies, which leads to a stronger 350 nm luminescence in the tetragonal nano-ZrO_2 than in the bulk sample. As the temperature is increased, the intensity of the 350 nm

* To whom correspondence should be addressed. E-mail: lib020@ciomp.ac.cn (B. Li), xwang@georgiasouthern.edu (X. Wang).
† Chinese Academy of Sciences.
‡ Georgia Southern University.
§ School of Science, Dalian Nationalities University, Dalian 116600, China.

10.1021/jp8103497 CCC: $40.75
Published on Web 07/14/2009

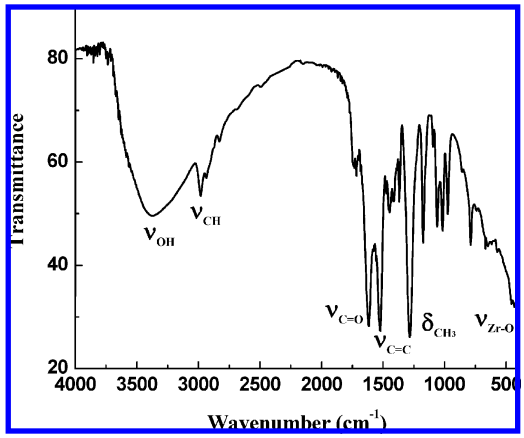

Figure 1. FT-IR spectrum of PZO.

emission decreases, and the 470 nm phosphorescence enhances in the phase transition process.

2. Experimental Section

2.1. Sample Preparation. PZO was synthesized via the one-pot reaction.[15] In the presence of triethylamine, the reaction of $ZrOCl_2 \cdot 8H_2O$ with ethyl acetoacetate yielded PZO as white powders according to the following equation

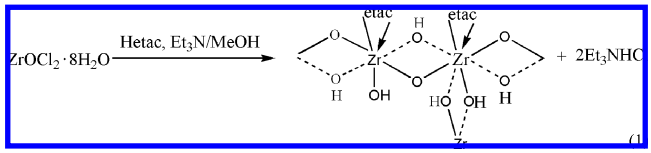

(1)

Successful synthesis of PZO can be verified by the Fourier transform infrared spectroscopy (FT-IR) spectrum.[15] Figure 1 shows the FT-IR spectrum with peaks at 3000 cm^{-1} (ν_{CH}), 1620 cm^{-1} ($\nu_{C=O}$), 1520 cm^{-1} ($\nu_{C=C}$), and 1280 cm^{-1} (δ_{CCH3}), respectively, corresponding to the absorption of the etac group. Another peak at 3400 cm^{-1} is the absorption of the OH group. The absorption band at 450 (ν_{Zr-O}) can be attributed to the Zr−O vibrations. The obtained PZO is stable to condensation and soluble in methanol, acetone, and tetrahydrofuron. It was dissolved in acetone, and then tetrabutyl titanate (TBT) was added to the solution with a concentration (C_{Ti}) of 0.1 mol % in relation to the Zr content. The mixture was maintained at 80 °C until the solvent was completely removed. The obtained crystalline was packed into alumina crucibles and annealed at 700, 900, 1000, and 1100 °C for 3 h in air.

2.2. Measurements. Structural characterization was analyzed by X-ray diffraction (XRD, Rigaku D/max-IIB) spectra with the Cu Kα line of 0.15405 Å. Morphology of products was observed by a HITACHI-4800 scanning electron microscope (SEM) equipped with an energy-dispersive X-ray spectrum (EDX).

Photoluminescence (PL) and PL excitation (PLE) spectra as well as phosphorescence decay curves were collected using a Hitachi F-4500 fluorescence spectrophotometer (resolution, 0.2 nm) equipped with a 150 W Xe lamp as the excitation source. Phosphorescence was detected after irradiation by 280 nm ultraviolet (UV) light for 5 min. Luminescent lifetime was measured with a 266 nm laser generated from a pulsed Nd:YAG (aluminum garnet) laser combined with a fourth harmonic generator. All measurements were carried out at room temperature.

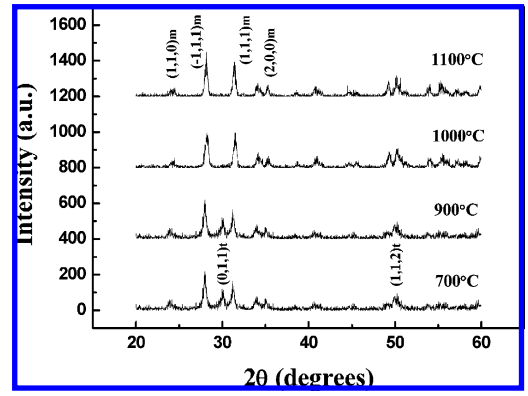

Figure 2. XRD patterns for nanocrystalline ZrO_2:Ti at different annealing temperatures.

3. Results and Discussion

3.1. Phase Transition and Morphology. Typical X-ray diffraction (XRD) patterns of synthesized nanocrystalline ZrO_2 for four different annealing temperatures are presented in Figure 2. For the sample annealed at 700 °C, characteristics of the monoclinic structure are presented with peaks centered at 28.40° $(-1, 1, 1)_m$, 31.40° $(1, 1, 1)_m$ and 35° $(2, 0, 0)_m$, respectively. Some weaker peaks resulting from the $(0, 1, 1)_t$ and $(1, 1, 2)_t$ reflections of tetragonal ZrO_2 are also observed. This indicates that tetragonal and monoclinic phases exist in the sample annealed at 700 °C. The sample annealed at 900 °C shows similar behavior to that annealed at 700 °C, except less amount of tetragonal phase is found, which implies a dominant monoclinic phase for the sample or some phase transition from tetragonal to monoclinic. The tetragonal phase is no longer detectable when the sample is heated at 1000 °C or higher, suggesting a complete phase transformation to monoclinic ZrO_2. Crystallinity of the monoclinic from ZrO_2 is improved as the annealing temperature increases.

The stability of the tetragonal phase in bulk ZrO_2 has been attributed to the presence of oxygen vacancies, which can be generated at higher temperatures, under reduced oxygen partial pressure, or by doping trivalent impurities. In nanocrystalline powders with very high specific surface area, more than 50% of the total atoms reside on the surface.[16] As a result of the size effect, a greater number of metal−oxygen bonds become weaker, which results in desorption of the lattice oxygen ions, creating a greater number of oxygen vacancies. The stabilization of the tetragonal structure in the ZrO_2 nanocrystallite at low temperatures below a critical size is due to the generation of excess oxygen vacancies as a result of the "nanoparticle size effect".[17,18]

SEM images and EDX spectra of nanocrystalline ZrO_2 sintered at 700 and 1100 °C are shown in Figure 3. A very ordered zirconia is obtained using the one-pot reaction. The sample annealed at 700 °C (tetragonal and monoclinic phases coexist) is composed of particles with an average size around 30 nm. Even sintered at temperature above 1000 °C (1100 °C), the sample (monoclinic phase) still has the ordered structure and relatively uniform size of around 100 nm. The improved morphology properties for the one-pot reaction with respect to the other methods (such as the sol−gel process,[12,19] forced hydrolysis,[20] and hydrothermal method[21]) is due to the immobilization of Zr and O homogeneity in the polymeric long-chain structure (see the structure in eq 1). EDX results (Figure 3c,d) confirm the presence of Zr, O, and C in the samples. The carbon impurity is primary from the Hetac group in the chain structure of PZO.

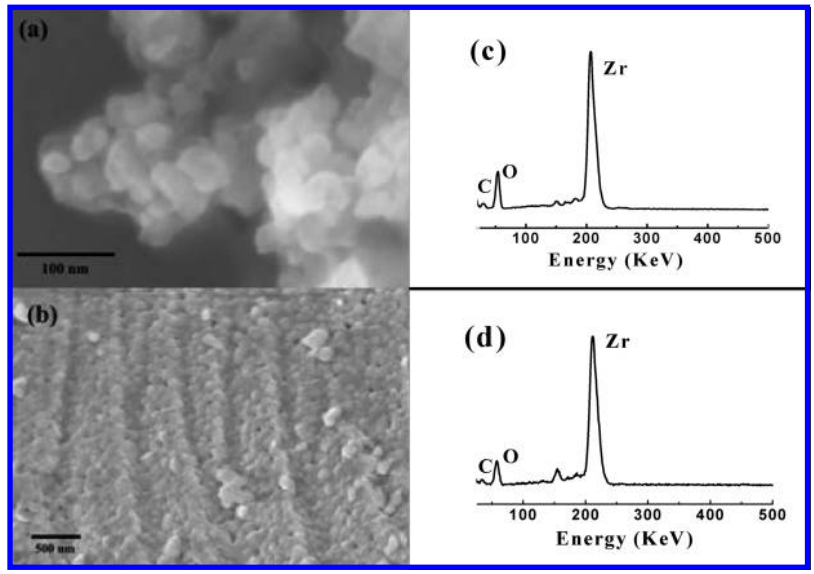

Figure 3. SEM image (a) and EDX (c) for nanocrystalline ZrO_2:Ti sintered at 700 °C as well as the SEM image (b) and EDX (d) for nanocrystalline ZrO_2:Ti sintered at 1100 °C.

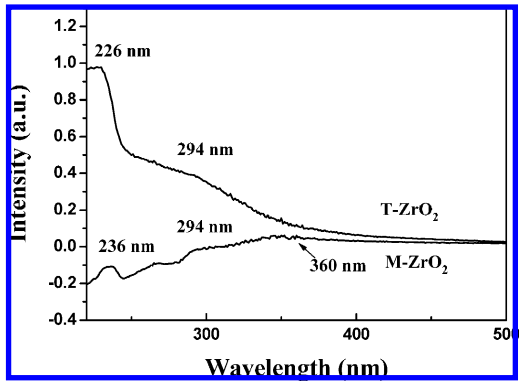

Figure 4. Absorption spectra of the tetragonal and monoclinic phase nano-ZrO_2 samples sintered at 700 and 1100 °C.

3.2. Photoluminescence Properties. Luminescence properties of ZrO_2 have been reported, but there is still a lack of clarification for the luminescent mechanisms in ZrO_2.[11,22−25] Harrison et al. first assumed that the luminescent center is constituted by a Zr^{4+} ion in an asymmetric site surrounded by oxygen ions.[23] This idea of a self-activated emission was rejected, and the luminescence from ZrO_2 was thought to be related to defects and/or impurities in the systems.[24−27] After investigating the photoluminescence and thermoluminescence of the undoped and Ti-doped (nanocrystalline) ZrO_2, we believe that photoluminescence and phosphorescence originate from the recombination of electrons trapped by oxygen vacancies and holes created in the valence band, and the Ti^{3+} ion substituting for Zr^{4+} is assumed to be the luminescent center.[11] The oxygen vacancy served as the F center, and the electrons trapper greatly affects the luminescent properties in the ZrO_2. The nanocrystalline ZrO_2:Ti exhibits a longer persistent time compared to that of the bulk because of the excess oxygen ion vacancies due to the large surface-to-volume ratio in the nanoparticles.[28]

The absorption spectra of the tetragonal and monoclinic phase nano-ZrO_2 samples sintered at 700 and 1100 °C are shown in Figure 4.The absorption band centered at 226 nm in the nano-ZrO_2, where the tetragonal phase is the major component, corresponds to the host absorption. This band is red-shifted to be 236 nm for monoclinic phase nano-ZrO_2. This red shift is produced by the decrease of the band gap caused by the stabilization of the tetragonal crystalline phase at room temperature.[29] The absorption bands centered at 294 and 360 nm are due to Ti^{3+} excited states.

Figure 5a shows the excitation and emission spectra of the tetragonal nano-ZrO_2 annealed at 700 °C. The excited spectrum presents three peaks centered at 235, 290, and 375 nm, which are associated with the absorptions of tetragonal zirconia in Figure 4. One band centered at 235 nm (5.3 eV) resulted from electron transfer from valence band (VB) to conduction band (CB) of the ZrO_2 host. The other two bands centered at 300 and 375 nm originated from electron transfer from the VB to the local midgap states, which are singly occupied oxygen vacancies (i. e., F^+ centers). The emission spectrum shows two broad bands centered at 350 and 470 nm. The 350 nm emission is attributed to compensating oxygen vacancies.[30] Excitation using electrons with energy exceeding the zirconia band gap produces electron−hole pairs. Electrons are trapped by the oxygen vacancies, creating F centers. Then the recombination of F centers with holes creates the excited states of the emitter. These excited emitters transfer to the ground state giving the 350 nm emission. When the electrons promoted to the VB are trapped by the oxygen vacancies, the thermal energy at ambient temperature causes the detrapping of the trapped electrons to the initial state of luminescence center Ti^{3+} and recombined with the holes trapped in the Ti^{3+} luminescence center, hence leading to the 470 nm blue-green phosphorescence.[28] The mechanism of the phosphorescence can be formulated in detail using a simplified scheme as shown in Figure 5b.

The emission intensity of Ti-doped nano-ZrO_2 is measured under excitation 280 nm as shown in Figure 6. As the temperature is increased, the intensity of the 350 nm emission decreases, and the 470 nm emission increases greatly. The tetragonal phase is stabilized at room temperature due to the presence of oxygen vacancies as a result of the "nanoparticle size effect". The generation of excess oxygen vacancies can greatly enhance the 350 nm luminescence of tetragonal phase nano-ZrO_2, which is not observed in the bulk sample sintered at the same temperature.[11] As the temperature is increased, nano-ZrO_2 shows a decrease at 350 nm luminescence due to the decrease of oxygen vacancies caused by the phase transformation from tetragonal to monoclinic. However, the 470 nm emission intensity is increased greatly with a decrease in the

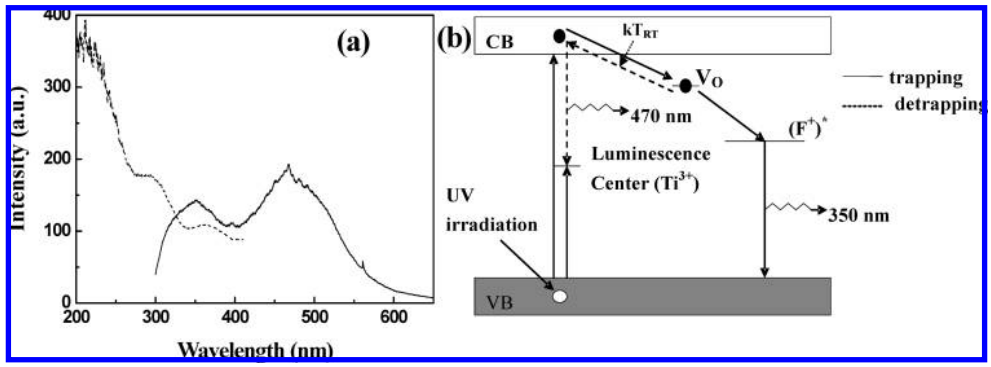

Figure 5. Excitation and emission spectra (a) and schematic diagram showing the possible defects and emission process (b) of tetragonal nano-ZrO_2 annealed at 700 °C.

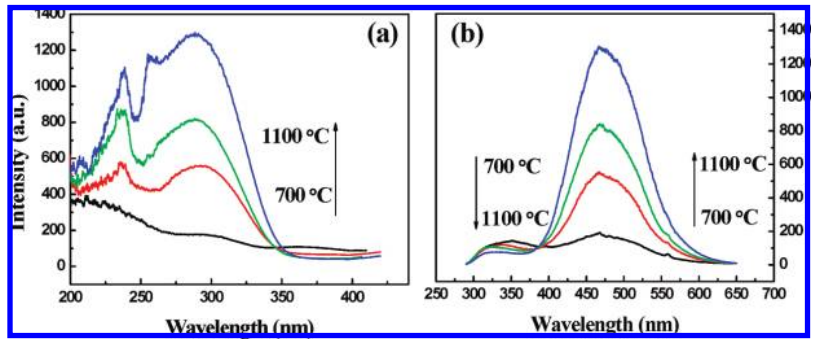

Figure 6. Excitation (a) and emission (b) spectra for nanocrystalline ZrO_2:Ti sintered at different temperatures.

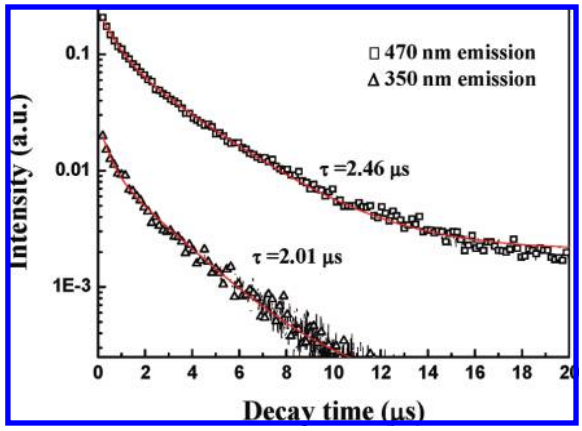

Figure 7. Decay curves for the two emissions from nanocrystalline ZrO_2 (350 and 470 nm).

oxygen vacancies, which may quench the luminescence and trap electrons or holes generated by UV excitation as shown in Figure 6b. The oxygen vacancy defects quench the emission because they could compete with activators and trap the excitation energy through nonirradiation transitions. Therefore, excess oxygen vacancies decrease in the phase transformation resulting in an increase luminescence at 470 nm. The corresponding 235 nm excitation band in the excitation spectrum is reduced, and the 290 nm excitation band is enhanced as shown in Figure 6a.

The decay curves for the two emissions from nanocrystalline ZrO_2 (350 and 470 nm) are shown in Figure 7. Both of the luminescence decay curves can be fitted to a second-exponential function given as $I(t) = A_1 \exp(-t/\tau_1) + A_2 \exp(-t/\tau_2)$, where A_1 and A_2 are the fitting parameters, and τ_1 and τ_2 are the fast and slow components of the luminescent lifetimes, respectively. These fitting results revealed that the lifetime of the 350 nm emission in nanocrystalline ZrO_2 phosphor is 2.01 μs, and that of the 470 nm emission is 2.46 μs. All of the parameters of the decay curves are listed in Table 1.

As mentioned above, titanium, the impurity in the system, is responsible for the 470 phosphorescence. Although the carbon-related impurity is also detected by EDX (Figure 3), we do not believe carbon plays a role as the emission center. First, carbon impurities are present in the samples sintered at 700 and 1100 °C (as shown in the EDX spectra). It is well-known that impurities like hydrogen and/or carbon are involved in the sample prepared by the wet-chemical process. These impurities could be eliminated at high annealing temperatures. Carbon impurities can be removed above 600 °C. Carbon is still present in large concentrations (14%) from our samples sintered at 700 and 1100 °C. Carbon is assumed to exist in the octahedral interstitials in zirconia lattice as pure atoms to form ZrO_2C_x solid solutions, so the introduction of carbon into the ZrO_2 host matrix does not break the electroneutrality of the phosphor and does not create a new anion vacancy. Second, the PL lifetime of ZrO_2 prepared via the pechini-type sol−gel process annealed at 500 °C is determined to be 5.8 ns in which luminescence is attributed to the carbon impurities built into the −Zr−O−C−O−Zr− networks.[19] This lifetime is much shorter than both of the lifetimes in our sample. From the above results, we can

TABLE 1: Time-Resolved Intensity Decay Constants for the Two Emissions from Nanocrystalline ZrO_2

emission (nm)	A_1	τ_1	A_2	τ_2	$\langle\tau\rangle$	r^2
350	$0.011 \pm 0.439 \times 10^{-19}$	$2.307 \times 10^{-6} \pm 0.131 \times 10^{-23}$	$0.016 \pm 0.522 \times 10^{-19}$	$3.924 \times 10^{-7} \pm 0.879 \times 10^{-23}$	2.01	1
470	$0.130 \pm 0.41 \times 10^{-4}$	$6.443 \times 10^{-7} \pm 0.845 \times 10^{-9}$	$0.109 \pm 0.47 \times 10^{-4}$	$2.946 \times 10^{-6} \pm 0.304 \times 10^{-9}$	2.46	0.9991

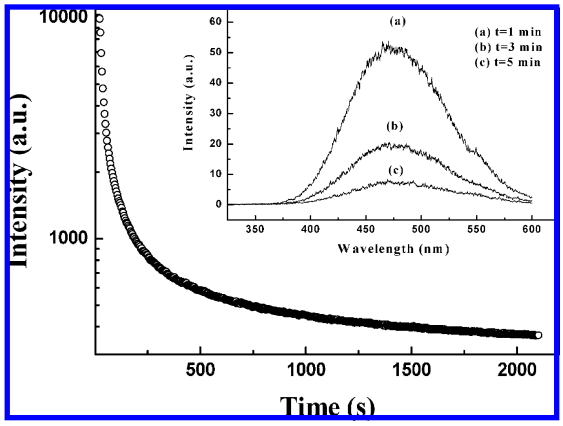

Figure 8. Afterglow intensity decay curve of phosphorescence at 470 nm in the ZrO_2 nanophosphor. Inset pattern is the afterglow spectra of this phosphor after the excitation source is switched off at different times (1, 3, and 5 min).

safely conclude that the carbon-related impurity could not play a role as emission centers, and the 470 nm phosphorescence in nanocrystalline zirconia is caused by the titanium impurity.

When titanium ions were introduced into the zirconium sites and sintered in a sealed crucible, mixture valence states of Ti (Ti^{4+}, Ti^{3+}) ions with a different ratio exist together in the samples. The Ti^{3+} ionic radius of 0.76 Å is closer to that of Zr^{4+} (0.79 Å) than that of Ti^{4+} (0.68 Å),[31] so the titanium ions tend to substitute for zirconium ions in the trivalent state rather than in the tetravalent state.[32] Phosphorescence lasting about 1 h appears only at the 470 nm emission, which proves the two emissions at 350 and 470 nm are of the different origins. Figure 8 shows the afterglow intensity decay of phosphorescence at 470 nm in the ZrO_2 nanophosphor. The afterglow from the sample can last for about 1 h after the removal of the UV light. As shown in the inset of Figure 8, the afterglow spectra are determined at different times (1, 3, and 5 min) after the excitation source is switched off. Only the afterglow at 470 nm is observed, and the shape and maximum peak position are similar with the normal emission spectrum. The same luminescence properties mean that the radiating centers in both cases are identical. Two Ti^{3+} ions substituting for a Zr^{4+} ion produces one oxygen vacancy for charge compensation. These anion vacancies, with the excess oxygen vacancies produced due to the nanoparticle size effect, are effective and deep traps for electrons generated in the CB during excitation, and the Ti^{3+} serves as the trapping center. Under UV irradiation, free electrons and holes are formed in the sample matrix. The electrons promoted to the VB can be trapped at the $V_O^{\cdot\cdot}$ defects located at local midgap states. The thermal energy at ambient temperature causes detrapping of electrons to the initial state of luminescence centers, and then recombining with holes trapped in the luminescence centers (Ti^{3+}) leads to the 470 nm blue-green phosphorescence.

4. Conclusion

In conclusion, effects of oxygen vacancies on phase transformation and photoluminescence properties of nanocrystalline ZrO_2 are reported in this paper. The tetragonal phase has been stabilized in nanocrystalline ZrO_2 at low temperature below a critical size. The phase transition process from tetragonal to monoclinic occurred in the annealing process. It is proposed that generation of excess oxygen vacancies within nanocrystalline zirconia is primarily responsible for room-temperature tetragonal phase stabilization and the phase transformation to monoclinic. The oxygen vacancy as the F center and the electrons trapper greatly affect the luminescent properties in ZrO_2 in the phase transition process. Two bands centered at 350 and 470 nm with different luminescent properties are observed in ZrO_2. The 350 nm emission is probably due to the excited-state F^+ transfer to the ground state. The 470 nm phosphorescence originated from the recombination of the detrapped electrons and holes in the Ti^{3+} luminescent center. The 350 nm emission is reduced, and the 470 nm phosphorescence in the monoclinic phase is greatly enhanced with an increase in annealing temperature, leading to phosphorescence for 1 h.

Acknowledgment. The authors gratefully thank the financial support from One Hundred Talents Project from the Chinese Academy of Sciences and the National Natural Science Foundation of China (Grants 20571071, 50872130, and 10574128).

References and Notes

(1) Ohta, K.; Yamada, K.; Shimizu, K.; Ozawa, T. *Solid State Ionics* **1982**, *3*−*4*, 443.
(2) Fork, D. K.; Fenner, D. B.; Connell, G. A. N.; Philips, J. M.; Geballe, T. H. *Appl. Phys. Lett.* **1990**, *75*, 1137.
(3) Jiang, S.; Shulze, W. A.; Stange, G. C. *J. Mater. Chem.* **1997**, *12*, 2374.
(4) Shukla, S.; Seal, S.; Vij, R.; Bandyopadhyay, S. *Nano. Lett.* **2003**, *3*, 0397.
(5) Leon, C.; Luci, M. L.; Santamaria, J. *Phys. Rev.* **1997**, *55*, 882.
(6) Yeh, W.; Patuwathavithane, C.; Zee, R. H. *J. Appl. Phys.* **1996**, *79*, 7809.
(7) Shukla, S.; Seal, S.; Vanfleet, R. J. *Sol.-Gel Sci. Technol.* **2003**, *27*, 119.
(8) Lu, K. *Mater. Sci. Eng.* **1996**, *16*, 161.
(9) Nitsche, R.; Rodewald, M.; Skandan, G.; Fuess, H.; Hahn, H. *Nanostruct. Mater.* **1996**, *7*, 535.
(10) Nitsche, R.; Winterer, M.; Hahn, H. *Nanostruct. Mater.* **1995**, *6*, 679.
(11) Cong, Y.; Li, B.; Lei, B.; Li, W. *J. Lumin.* **2007**, *126*, 822.
(12) Chang, S. M.; Doong, R. A. *J. Phys. Chem. B* **2006**, *110*, 20808.
(13) Pacheco, G.; Zhao, E.; Garcia, A.; Sklyarov, A.; Fripiat, J. J. *J. Mater. Chem.* **1998**, *8*, 219.
(14) Yang, P. D.; Zhao, D. Y.; Margolese, D. I.; Chmelka, B. F.; Stucky, G. D. *Nature* **1998**, *396*, 152.
(15) Abe, Y.; Tomioko, H.; Gunji, T.; Nagao, Y.; Misono, T. *J. Mater. Sci. Lett.* **1994**, *13*, 960.
(16) Uehara, M.; Barbara, B.; Dieny, B.; Stamp, P. C. E. *Phys. Lett. A.* **1986**, *114*, 23.
(17) Shukla, S.; Seal, S. *Int. Mater. Rev.* **2005**, *50*, 45.
(18) Oleshko, V.; Howe, J.; Shukla, S.; Seal, S. *J. Nanosci. Nanotechnol.* **2004**, *4* (7), 867.
(19) Lin, C.; Zhang, C.; Lin, J. *J. Phys. Chem. C* **2007**, *111*, 3300.
(20) Hu, M. Z. C.; Harris, M. T.; Byers, C. H. *J. Colloid Interface Sci.* **1998**, *198*, 87.
(21) Wu, J. M.; Wu, C. M. *J. Mater. Sci.* **1988**, *23*, 3290.
(22) Chernov, V.; Belykh, A.; Melendrez, R.; Barboza-Flores, M. *J. Non-Cryst. Solids* **2006**, *352*, 2543.
(23) Harrison, D. E.; Melamed, N. T.; Subbarao, F. C. *J. Electrochem. Soc.* **1963**, *110*, 23.
(24) Sarver, J. F. *J. Electrochem. Soc.* **1966**, *113*, 124.
(25) Iacconi, P.; Lapraz, D.; Caruba, R. *Phys. Status Solidi A* **1978**, *50*, 275.
(26) Brankova, T.; Bekiari, V.; Lianos, P. *Chem. Mater.* **2003**, *15*, 1855.
(27) Pifferi, A.; Taroni, P.; Torricelli, A.; Valentini, G.; Mutti, P.; Ghislotti, G.; Zanghieri, L. *Appl. Phys. Lett.* **1997**, *70*, 348.
(28) Cong, Y.; Li, B.; Wang, X.; Lei, B.; Li, W. J. *Electrochem Soc.* **2008**, *155*, K195.
(29) PaiVerneker, V. R.; Petelin, A. N.; Crowne, F. J.; Nagle, D. C. *Phys. Rev. B* **1989**, *40*, 8555.
(30) Petrik, N. G.; Taylor, D. P.; Orlando, T. M. J. *Appl. Phys.* **1999**, *85*, 6770.
(31) Weast, R. C.; *Handbook of Chemistry and Physics*, 46th ed.; Chemical Rubber Co.: Cleveland, OH, 1965/1966; p F117.
(32) Iacconi, P.; Lapraz, D.; Caruba, R. *Phys. Status Solidi A* **1978**, *50*, 275.

JP8103497